Supplementary Information

High-loading As single-atom catalysts harvested from wastewater towards efficient and sustainable oxygen reduction

Yangjun Luo[a,1], Yanwei Wang [a,1], Huijuan Zhang [a,b,1], Youyuan Wang[a,1], Jin Wan[a], Chuanzhen Feng[a], Lingmei Liu[a], Zaiping Guo[c*], Jian Li[a], Yu Wang[a,b*]

[a] State Key Laboratory of Power Transmission Equipment Technology, School of Chemistry and Chemical Engineering, Chongqing University, Chongqing, 400044, P. R. China

[b] College of Chemistry and Environmental Science, Inner Mongolia Normal University, Huhehaote, 010022, P. R. China

[c] School of Chemical Engineering and Advanced Materials, University of Adelaide, Adelaide 5005, Australia.

[1] These authors contribute equally

*E-mail: zaiping.guo@adelaide.edu.au; wangy@cqu.edu.cn

Supplementary Information:

1. Methods

Synthesis of RC support. In a typical procedure, 10 g potassium citrate tribasic monohydrate ($K_3C_6H_5O_7 \cdot H_2O$) precursors were transferred to a tube furnace[1]. The furnace was heated to 800 °C for 1 h with a continuous flow of argon (Ar) gas at 70 sccm. The black products were stirred in 0.5 M H_2SO_4 for 12 h to remove the metal impurities. The sample was then washed with deionized water and ethanol, respectively. After drying at 60 °C, the regular carbon (RC) support was obtained.

Synthesis of As-DC1-1050, As-RC1-1050, As-DC2-1050 and DC support. First, 150 mg RC support, 1.0 mmol of zinc nitrate hexahydrate and 20 mmol of α-D-glucose were dispersed in 10 mL of deionized water and sonicated for 40 min. The resulting slurry was washed with deionized water and dried to obtain a black powder. 60 mg of the resulting powder was placed uniformly in thin layers on a combustion boat and then transferred to the downstream end of the tube furnace. 240 mg of $NaAsO_2$ was placed on another combustion boat and was transferred upstream to the tube furnace. The two boats were spaced 1-2 cm apart and one end was mechanically cut off to allow unobstructed passage of the gas.

Secondly, single-atom As was loaded adjacent to the defects formed by the evaporation of zinc via the CVD method. To allow relatively gentle evaporation/decomposition of $NaAsO_2$, the temperature was raised to 820 °C for 40 minutes with a continuous flow of Ar gas at 70 sccm. The temperature was then further increased to 910 °C (around the boiling point of zinc) for 30 min and finally to 1050 °C for 30 min. The above samples were thoroughly washed with hydrochloric acid and deionized water to remove the effects of residual zinc to obtain As-DC1-1050. Notably, it is necessary to place an alkaline solution such as NaOH to treat the arsenic-containing tail gas to protect the safety of experimenters. In addition, good protective equipment such as gloves and masks should be worn when moving solid drugs such as $NaAsO_2$. Similarly, As-RC1-1050 was synthesized without the addition of zinc nitrate hexahydrate. As-DC2-1050 was also synthesized without the addition of α-D-glucose. DC support was also synthesized without the addition of $NaAsO_2$.

Synthesis of Se-DC1-1050, I-DC1-1050, P-DC1-1050 and Br-DC1-1050. Similarly, $NaAsO_2$ was also replaced with SeO_2, I_2, NaH_2PO_2 and Br_2 to synthesize Se-DC1-1050, I-DC1-1050, P-DC1-1050 and Br-DC1-1050. Notably, to facilitate the relatively gentle

evaporation of SeO_2, the temperature was raised to 690 °C (around the SeO_2 boiling point temperature) for 40 min under the Ar atmosphere. To allow for relatively gentle evaporation of I_2, the temperature was raised to 200 °C (around the I_2 boiling point temperature) for 40 min under the Ar atmosphere. Similarly, NaH_2PO_2 was raised to 230 °C and Br_2 was raised to 60 °C. The remaining conditions were identical to those for the synthesis of As-DC1-1050. Since Br_2 is a liquid, Br_2 was poured into a crucible as a source of bromine.

Research on degradation inhibition. According to our previous work, to collect an adequate amount of As-DC1-1050 after the accelerated durability test (ADT), the glassy carbon (GC) electrode was replaced by a platinum sheet (PS) electrode with an effective area of 2 cm × 2 cm^2. The loading of As-DC1-1050 on the PS electrode was 1.8-2.2 mg cm^{-2}. After 35,000 cyclic voltammetry (CV) cycles, As-DC1-1050 was scraped off and washed several times with ethanol and deionized water, then dried and collected. The catalyst was then heated to 400 ^oC for 30 min in H_2/Ar atmosphere to furnish As-DC1-1050-R1. Similarly, As-RC1-1050-R1 can be obtained with such an operation.

Catalyst characterizations. The X-ray photoelectron spectroscopy (XPS) analysis was carried out on an ESCALAB 250Xi (Thermo Fisher Scientific, USA) spectrometer with an Al Kα radiation source. The binding energies of As in As-DC1-1050 at different potentials were further analyzed with reference to a previous report[3]. The morphologies and X-ray energy dispersive spectroscopy (EDS) analyses of the As-based non-metal catalysts were characterized using an objective spherical aberration-corrected transmission electron microscopy (AC-TEM, FEI Titan ChemiSTEM) and TEM (Talos F200S and Super-X EDS), respectively. PANalytical X'Pert Powder and inductively coupled plasma optical emission spectrometer (ICP-OES 6300, USA) were used to collect the X-ray diffraction (XRD) patterns (Spectris Pte. Ltd, Netherlands) and the actual As loadings, respectively. A multistation surface and porosity analyzer max-II (MicrotracBEL, Japan) and Raman spectrometer equipped with laser (532 nm) in the wavenumber of 500-2500 cm^{-1} (Horiba Jobin Yvon S.A.S.) were performed to characterize the As-based non-metal catalysts. The X-ray absorption spectra of the As K-edge were processed and fitted with Athena and Artemis programs.

Electrochemical measurements. A three-electrode system (Model AFMSRCE) was

used to measure the ring and disk currents. A rotating ring-disk electrode (RRDE) with an outside diameter of 5.50 mm or a GC electrode with a dimension of 5 mm served as the working electrode. The electrochemical LSV and CV data were quantified to evaluate ORR performance. A carbon rod was used as counter electrode and Ag/AgCl (3M KCl solution) was worked as reference electrode. According to the following formula, all reported potentials were calibrated against the reversible hydrogen electrode (RHE) reference: $E_{RHE}=E_{Ag/AgCl}+0.059pH+0.197$. 5.5 mg As-DC1-1050 or 1.5 mg 20 wt% Pt/C was dispersed in a mixture of ethanol (980 μL) and 5 wt% Nafion (20 μL) by ultrasonication for at least 35 min. 10 μL of prepared catalyst ink was transferred to the working electrode. Voltage cycling between 0.6 and 1.0 V was used to conduct the ADT of the As-DC1-1050 in O_2-saturated 0.1 M KOH. Electrochemical impedance spectroscopy (EIS) measurements were conducted in O_2-saturated electrolyte solutions with an alternating current perturbation voltage of 5 mV in the frequency range of 1000 kHz to 0.1 Hz[3-5]. The potential of the ring electrode was maintained at 1.2 V (vs. RHE).

Quasi-operando XPS of As-DC1-1050 working at applied potentials. According to the previous report[3], the back side of the Si_3N_4 window where the catalyst was deposited on the Au/Ti layer faced into the interior of the electrochemical cell. An Ag/AgCl reference electrode was placed in the Luggin capillary and a carbon rod was prepared as a counter electrode. To avoid Cl^- contamination, the Ag/AgCl electrode was fixed on one side of the cell. The As-DC1-1050 catalyst was placed in 0.1 M O_2-saturated electrolyte and then the reactor was vacuumized. At each set potential, the electrode was first polarized for 4 min until it was stable, and then XPS signals were collected at different applied potentials (0.5 V，0.7 V, 0.9 V, 1.1 V vs. RHE).

Electrochemical measurements for zinc-air battery. Electrochemical performance tests were performed on a self-assembled ZAB. 6 mg of catalyst (As-DC1-1050 or 20% Pt/C) and 20 uL of a 5 wt% Nafion solution were dispersed into 580 uL of ethanol solution by sonication for 45 min. Afterwards, the ink was transferred to hydrophobic carbon paper (TGPH 120) with a catalyst loading of 1 mg cm^{-2}. Polished zinc foil and 6.0 M KOH containing 0.2 M zinc acetate were used as anode and electrolytes for ZAB, respectively.

Electrochemical measurements for fuel cells. As-DC1-1050 and 20% Pt/C were scattered in a compound solution of FAA-3 ionomer (5 wt%), isopropanol and deionized

water to formalize cathodic and anodic inks (4 mL) of HOFCs, respectively. The ink was sonicated for 30-50 min and then uniformly sprayed on both sides of an anion exchange membrane with an active area of 4 cm^{-2}. The catalyst loadings were 3.5 mg cm^{-2} of As-DC1-1050 for the cathode and 0.4 mg cm^{-2} of Pt/C for the anode. The capability of assembled HOFCs was analyzed at Riror RG100 operating at 65 °C. Constant H_2 (100 sccm) and O_2 (200 sccm) flow rates were delivered with a humidity of 100% at a back pressure of 1.0 bar. The As-DC1-1050 cathode was also operated at a practical fuel cell voltage of 0.67 V for 290 h to investigate its durability. A constant flow of hydrogen (100 sccm) and air (200 sccm) was passed into HOFCs at 100% humidity in the stability tests. Then As-DC1-1050-290 was then heated to 400 °C for 30 min in H_2/Ar atmosphere. Next, the As-DC1-1050-290-R cathode continued to be operated at a constant voltage of 0.67 V.

Computational methods. First-principles calculations were carried out by the Vienna ab initio simulation package (VASP-5.4.4)[6]. The Perdew–Burke–Ernzerhof (PBE) version of the generalized gradient approximation (GGA) was employed for the exchange–correlation interaction[7]. Electron spin polarization was considered in all the calculations. During structure relaxation, the iterative convergence of the energy was set to 10^{-5} eV and each atom was fully relaxed until the residual forces were converged to 0.01 eV/Å. The energy cut-off was chosen as 450 eV. The partial carbon defect model calculated in this paper refers to the previous literature[8, 9]. A vacuum slab of 20 Å was utilized along the z-direction to avoid the mirror interaction between periodic images. Considering the porous configurations of the As-C-based non-metal catalysts, the van der Waals interaction was involved by using the empirical correction in the Grimme's scheme (DFT+D3)[7]. The Brillouin-zone integration was sampled by a *Γ*-centered 1 × 2 × 1 k-point mesh for structural relaxation, and a denser 2 × 4 × 2 mesh was used for the electronic property calculations, respectively.

2. Supplementary Figures.

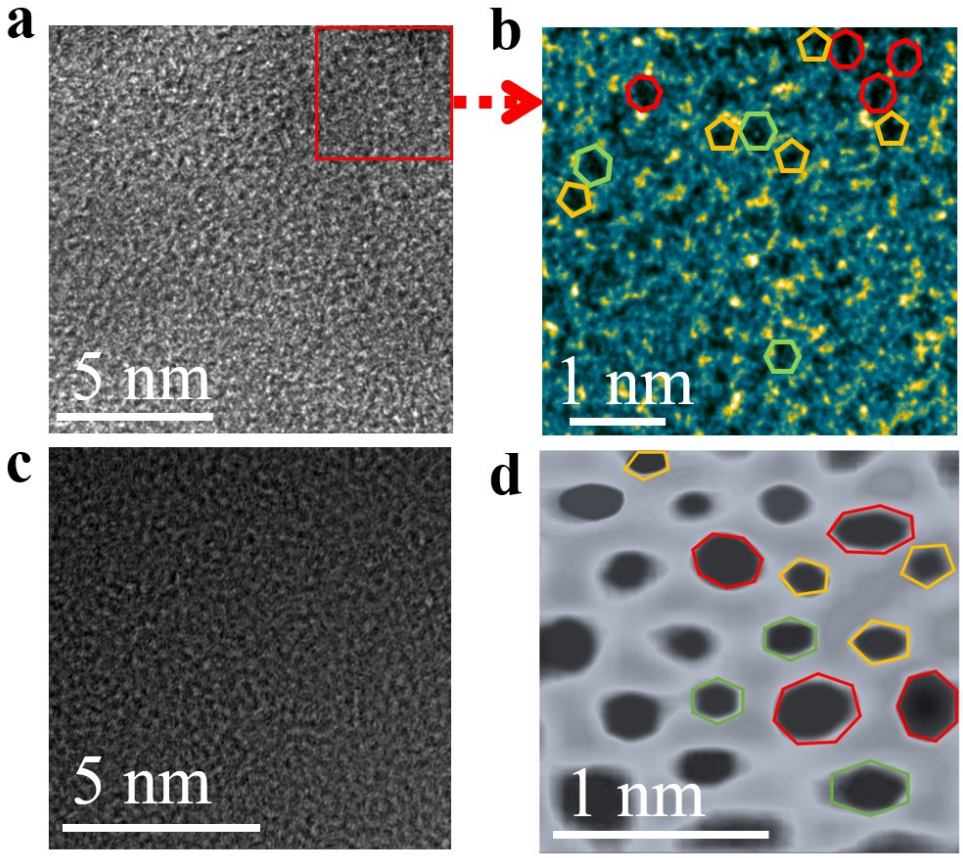

Figure S1. HAADF image of As-DC1-1050. Pentagons, hexagons and heptagons are marked in yellow, green and red respectively.

Figure S2. Optical pictures of the as synthesized As-DC1-1050.

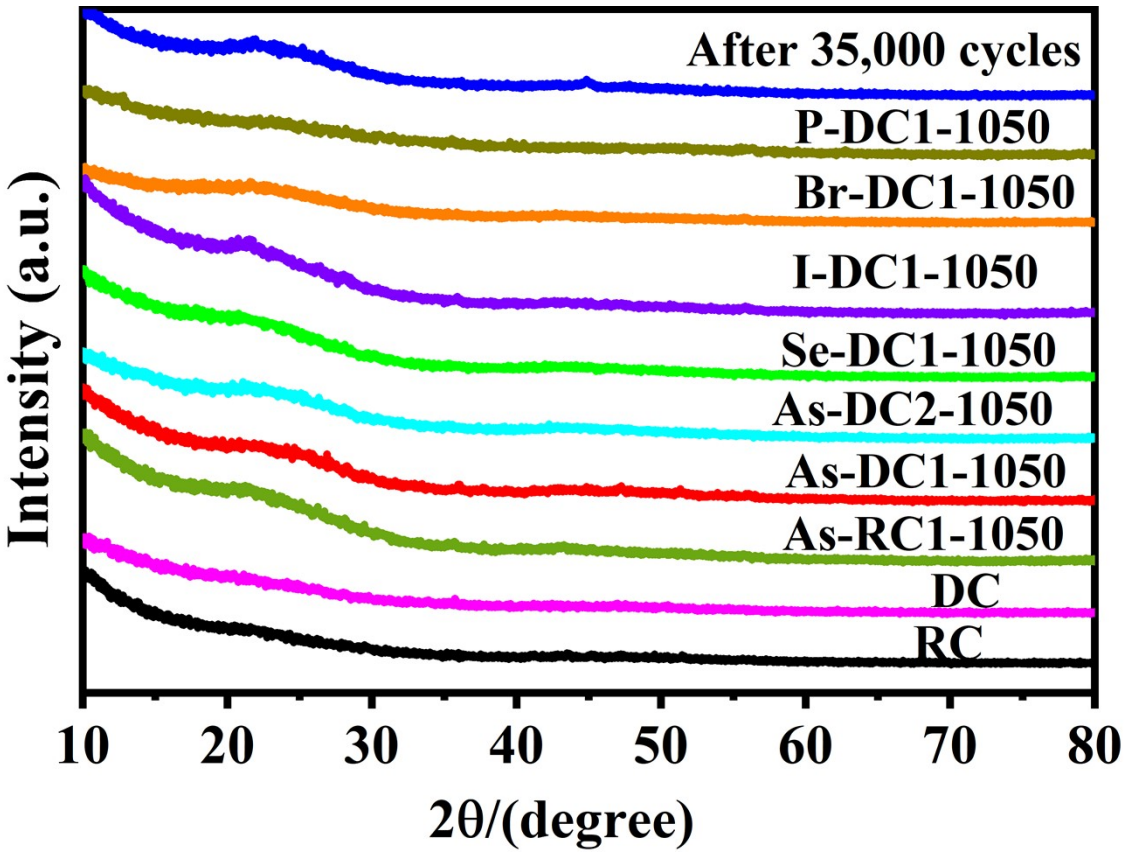

Figure S3. XRD patterns of the as synthesized RC, DC, As-RC1-1050, As-DC1-1050, As-DC2-1050, Se-DC1-1050, I-DC1-1050, Br-DC1-1050, P-DC1-1050 and As-DC1-1050 after 35,000 cycles.

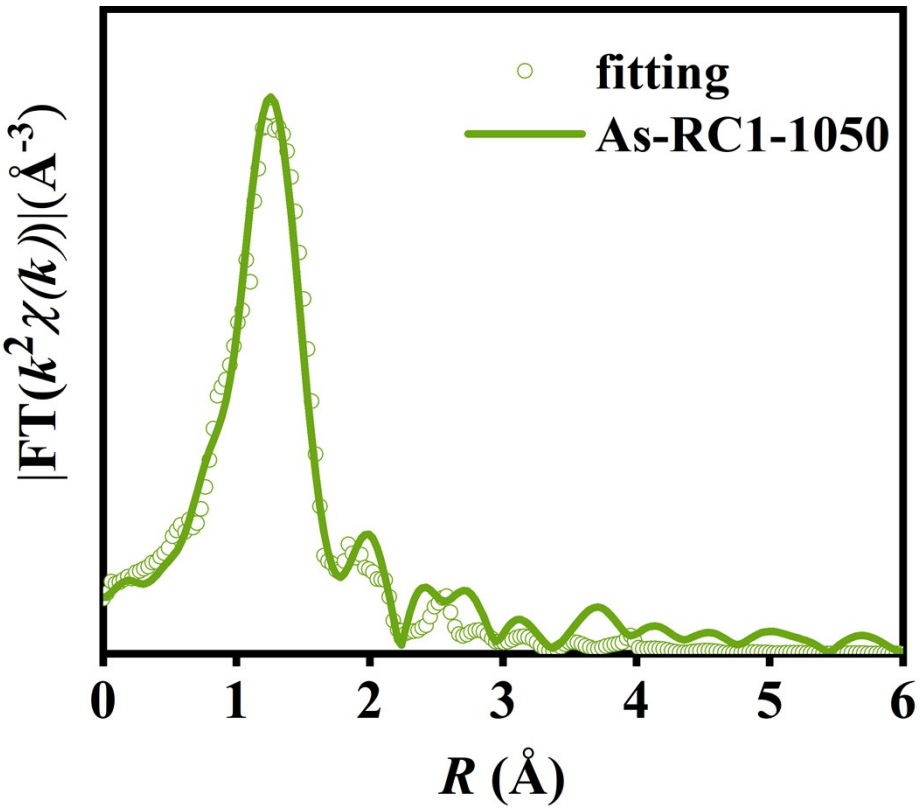

Figure S4. FT-EXAFS fitting curves of As K-edge for As-RC1-1050.

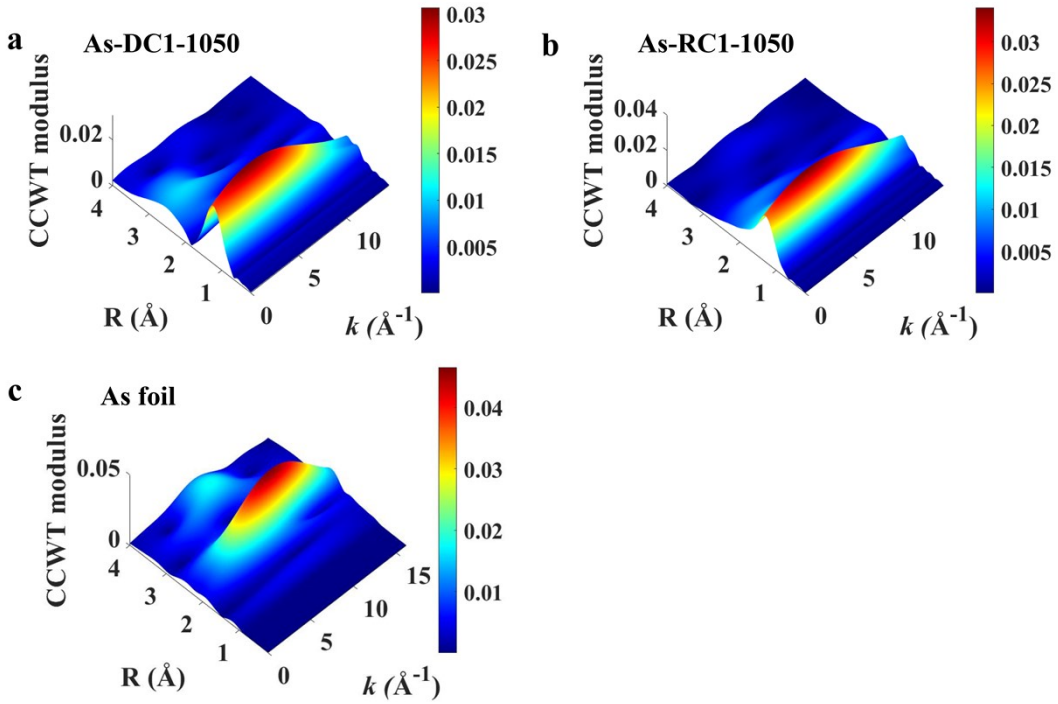

Figure S5. WT of the k^2-weighted EXAFS data of (a) As-DC1-1050, (b) As-RC1-1050 and (c) As foil.

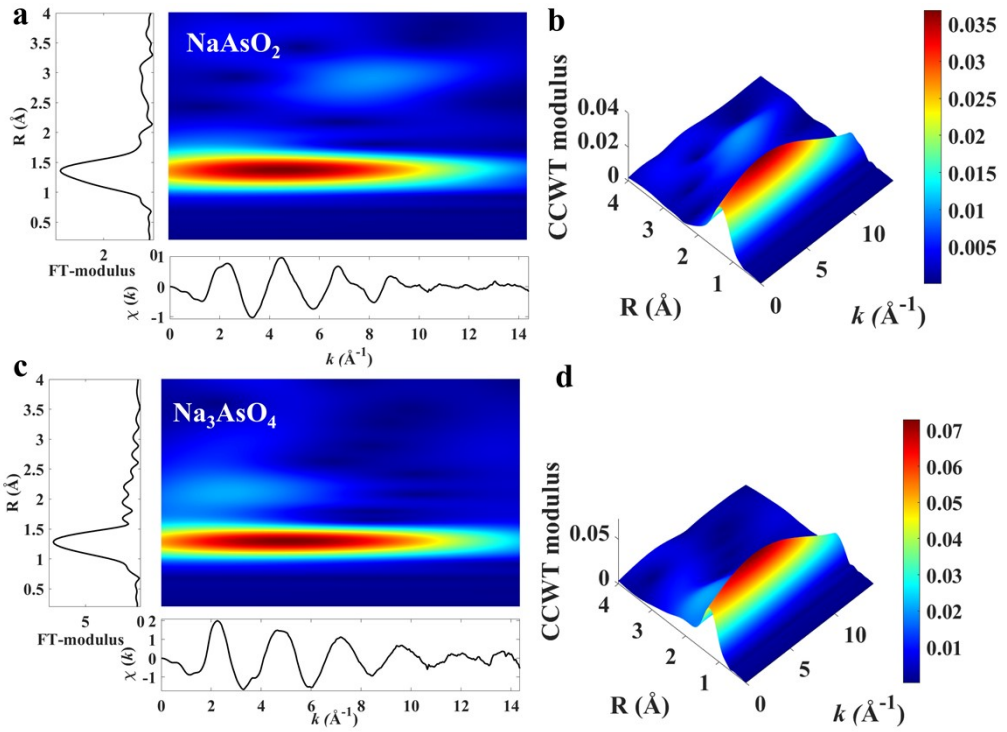

Figure S6. WT of the k^2-weighted EXAFS data of (a-b) $NaAsO_2$ and (c-d) Na_3AsO_4.

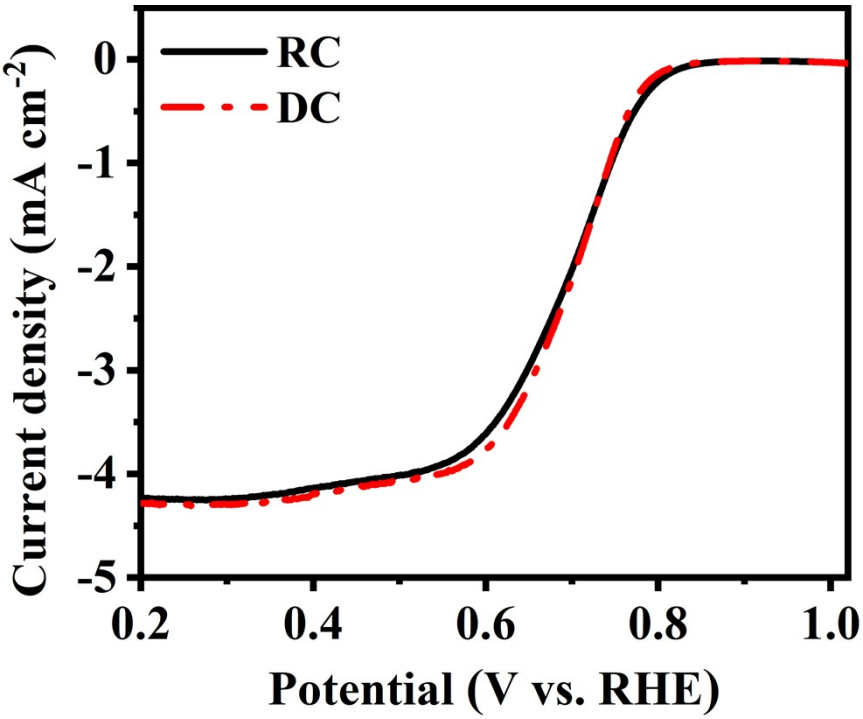

Figure S7. An oxygen reduction performance comparison of RC and DC in 0.1 M KOH.

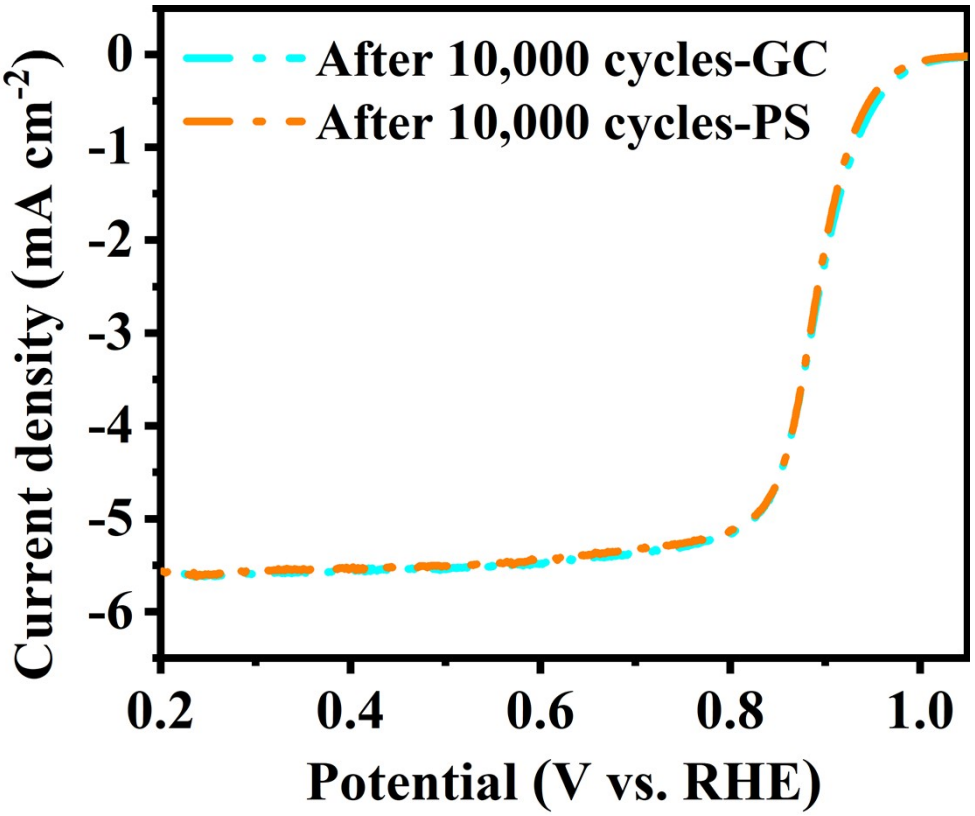

Figure S8. ORR polarization curves of As-DC1-1050 transferred to a glass carbon (GC) electrode and a platinum sheet (PS) electrode after 10,000 CV cycles, respectively.

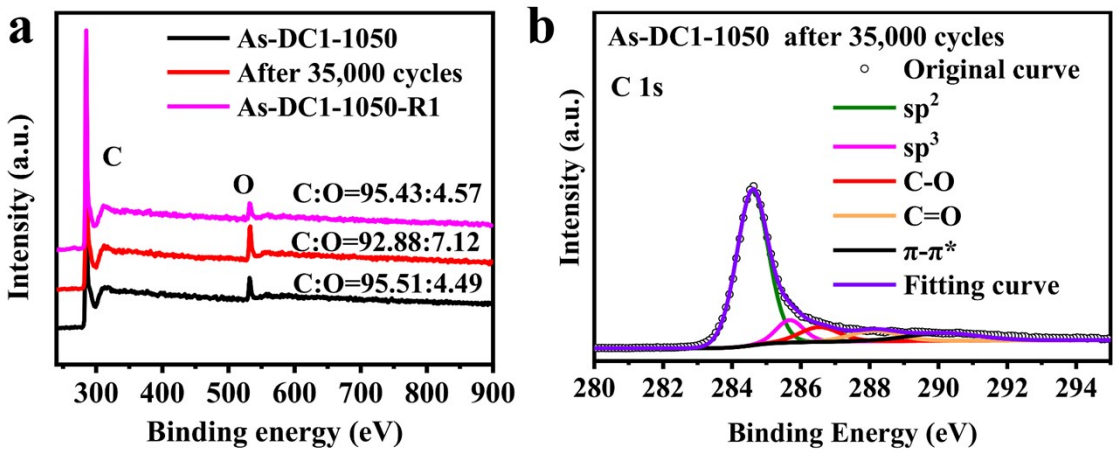

Figure S9. (a) XPS survey of As-DC1-1050, As-DC1-1050 after 35,000 cycles and As-DC1-1050-R1 samples. (b) Deconvoluted carbon 1s spectrum of As-DC1-1050 after 35,000 cycles.

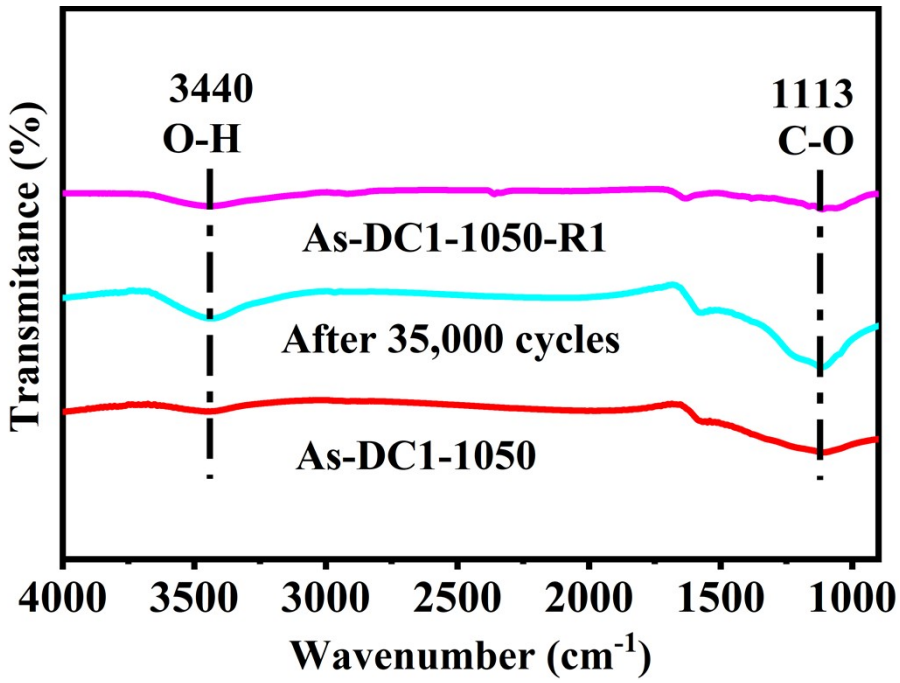

Figure S10. FT-IR spectra of As-DC1-1050, As-DC1-1050 after 35,000 cycles and As-DC1-1050-R1.

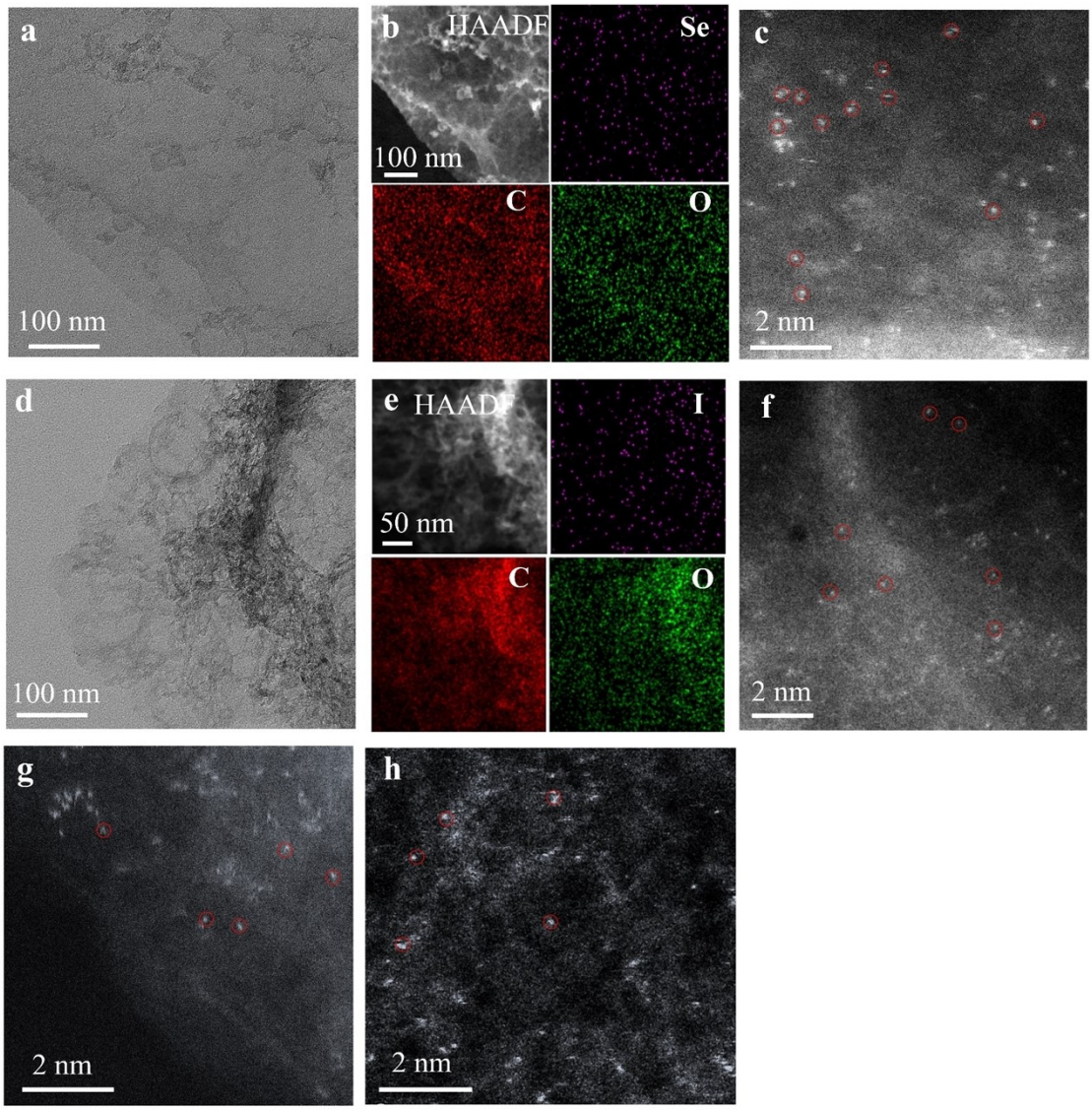

Figure S11. (**a**) TEM, (**b**) EDS images and (**c**) HAADF-STEM images of Se-DC1-1050. (**d**) TEM, (**e**) EDS images and (**f**) HAADF-STEM images of I-DC1-1050. HAADF-STEM images of (**g**) P-DC1-1050 and (h) Br-DC1-1050.

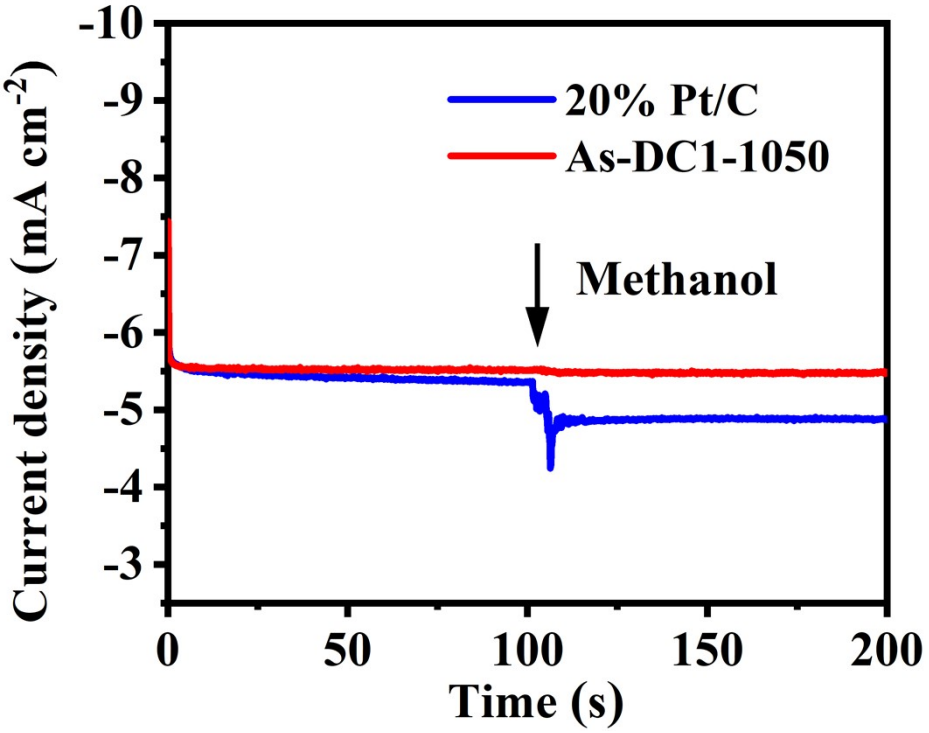

Figure S12. Methanol tolerance tests of 20% Pt/C and As-DC1-1050. Commercial Pt/C is known to show disappointing methanol tolerance in practice, with a 13.1% drop in current density after methanol addition. In contrast, the current density of the As-DC1-1050 does not change significantly after the addition of methanol, with an overall drop of only 2.2%, demonstrating its excellent methanol tolerance.

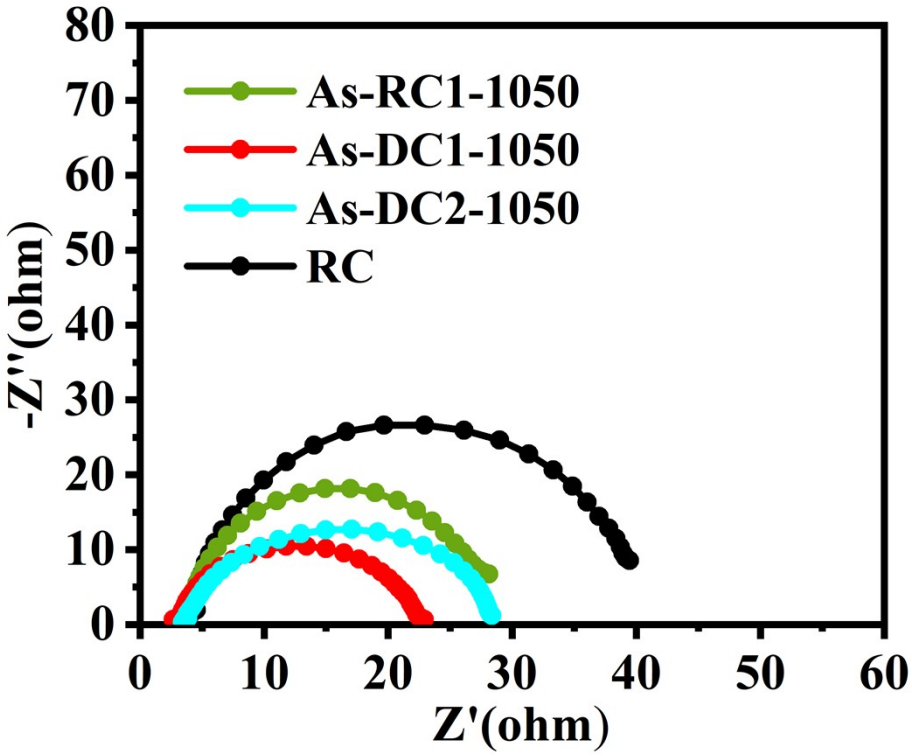

Figure S13. Electrochemical impedance spectroscopy curves of As-based non-metal catalysts in O_2-saturated 0.1 M $HClO_4$.

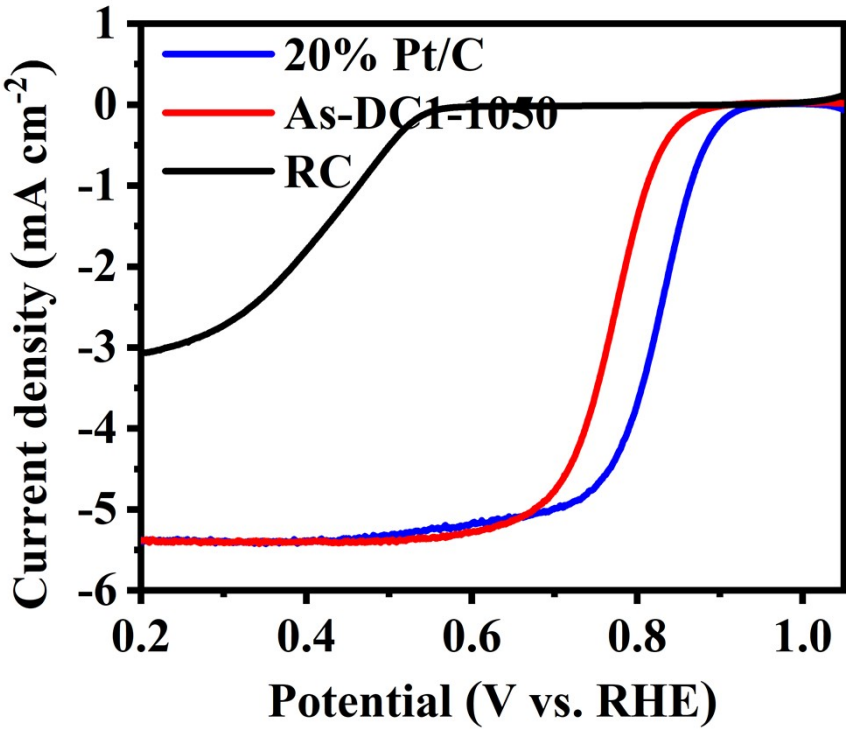

Figure S14. An oxygen reduction performance comparison of RC, 20% Pt/C and As-DC1-1050 in 0.1 M $HClO_4$.

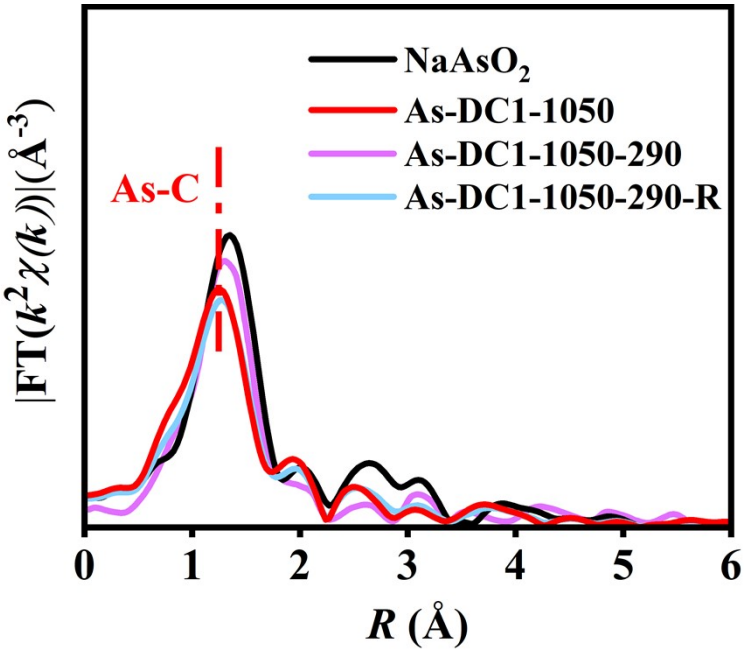

Figure S15. FT-EXAFS spectra of As-DC1-1050, As-DC1-1050-290, As-DC1-1050-290-R and $NaAsO_2$.

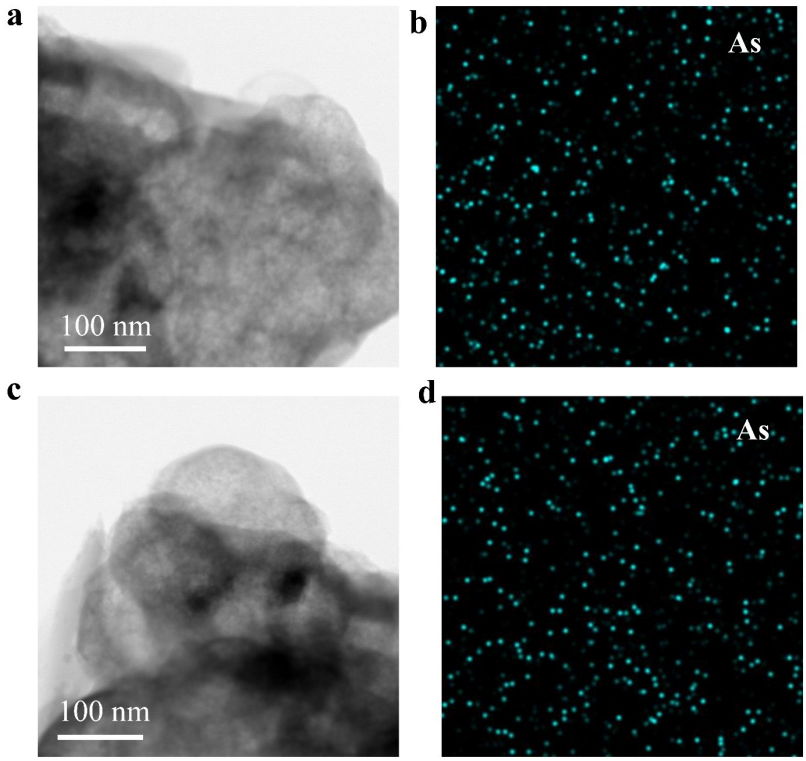

Figure S16. (a) TEM and (b) EDS images of As-DC1-1050-290. (c) TEM and (d) EDS images of As-DC1-1050-290-R.

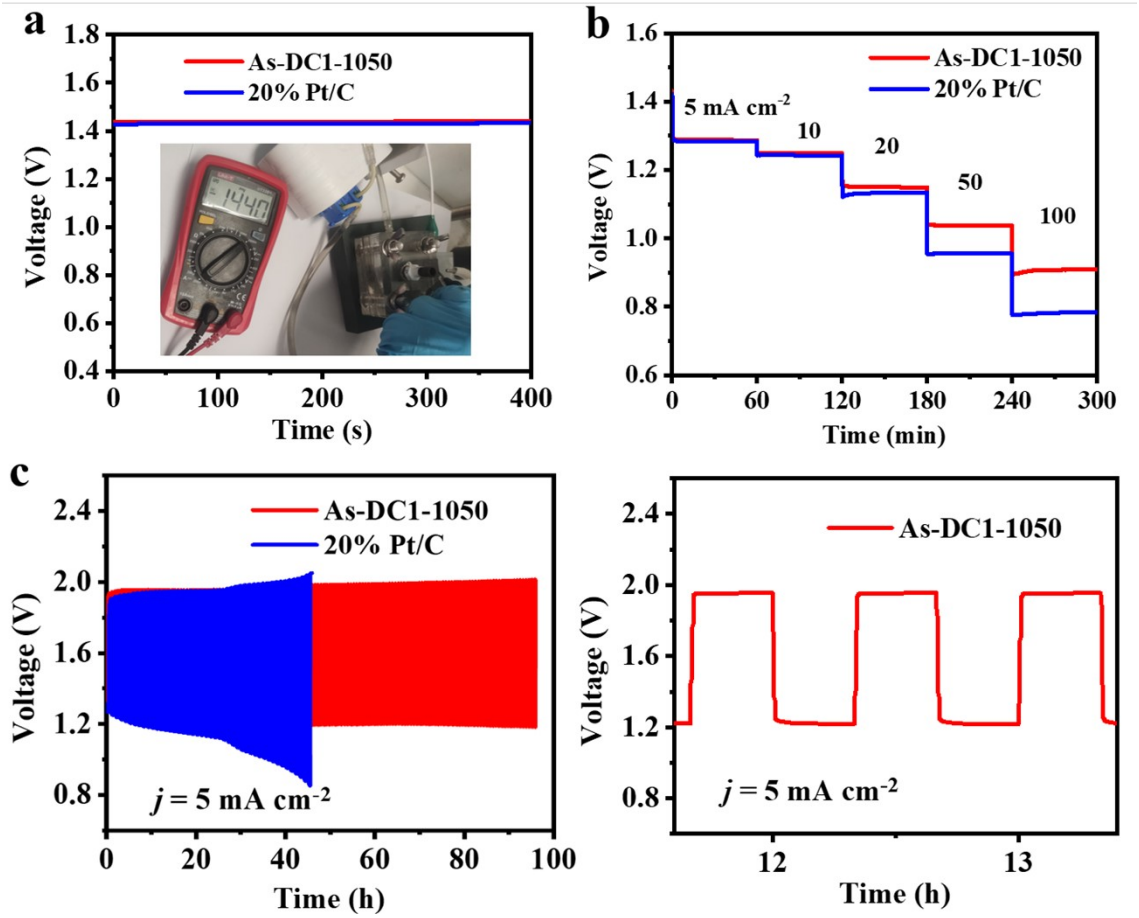

Figure S17. (a) Open circuit voltages, (b) rate capabilities and (c) galvanostatic cycling at 5 mA cm^{-2} of Zn-air battery using As-DC1-1050 and 20% Pt/C as the cathode catalyst.

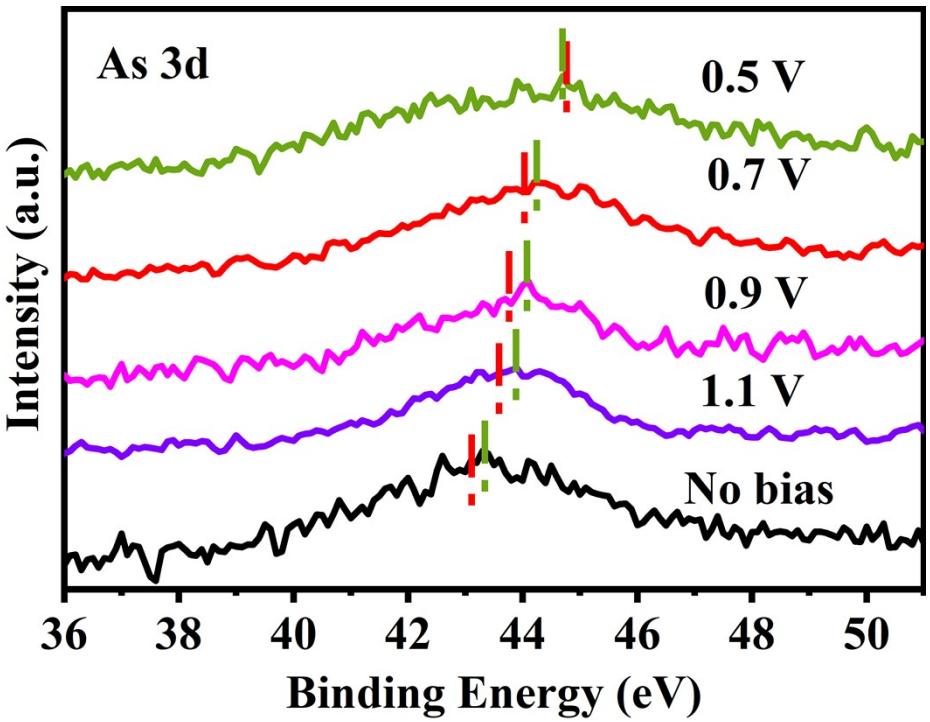

Figure S18. XPS of As-DC1-1050-290 at different potentials in 0.1 M $HClO_4$. The red and green dotted lines represent the binding energy positions of As in As-DC1-1050 and As-DC1-1050-290, respectively.

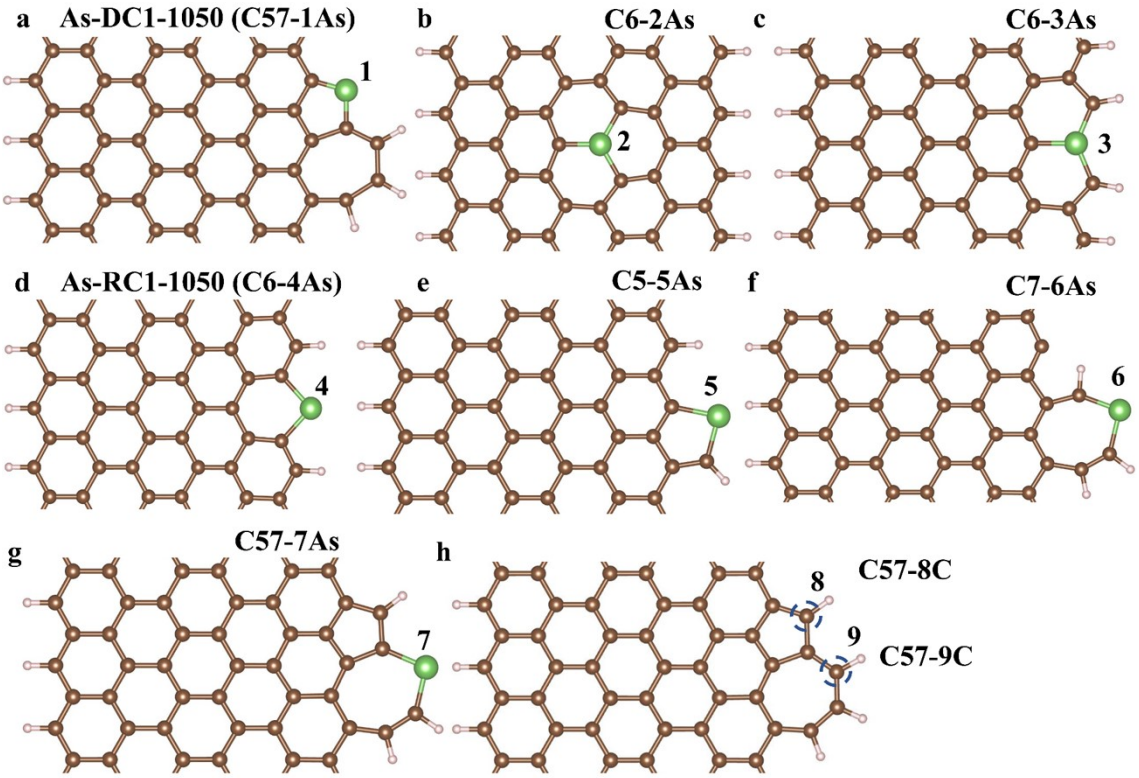

Figure S19. Different models for DFT calculations. (a) Arsenic at the edge site 1 of the adjacent five-carbon ring and seven-carbon ring (C57-1As). (b) Quaternary arsenic in the bulk phase (C6-2As). (c) Quaternary arsenic on the edge (C6-3As). (d) Pyridine arsenic (C6-4As). (e) Pyrrolic arsenic (C5-5As). (f) Arsenic at the edge site 6 of the seven-carbon ring (C7-6As). (g) Arsenic at the edge site 7 of the adjacent five-carbon ring and seven-carbon ring (C57-7As). (h) Carbon at the edge site 8 and 9 of the adjacent five-carbon ring and seven-carbon ring (C57-8C and C57-9C). The carbon, hydrogen and arsenic elements are denoted in brown, pink and green balls, respectively.

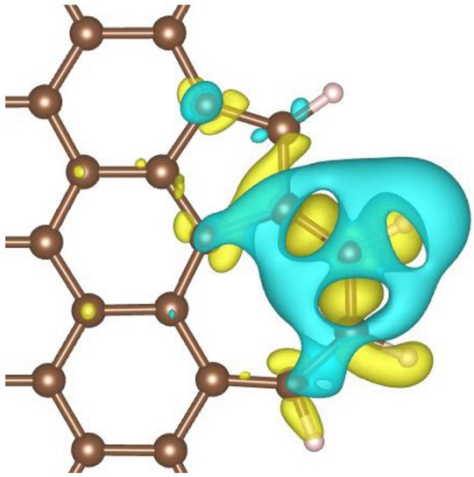

Figure S20. Differential charge density of C57-9C. Cyan and yellow represent electron depletion and accumulation; the iso-surface value is 0.003 e $Å^{-3}$.

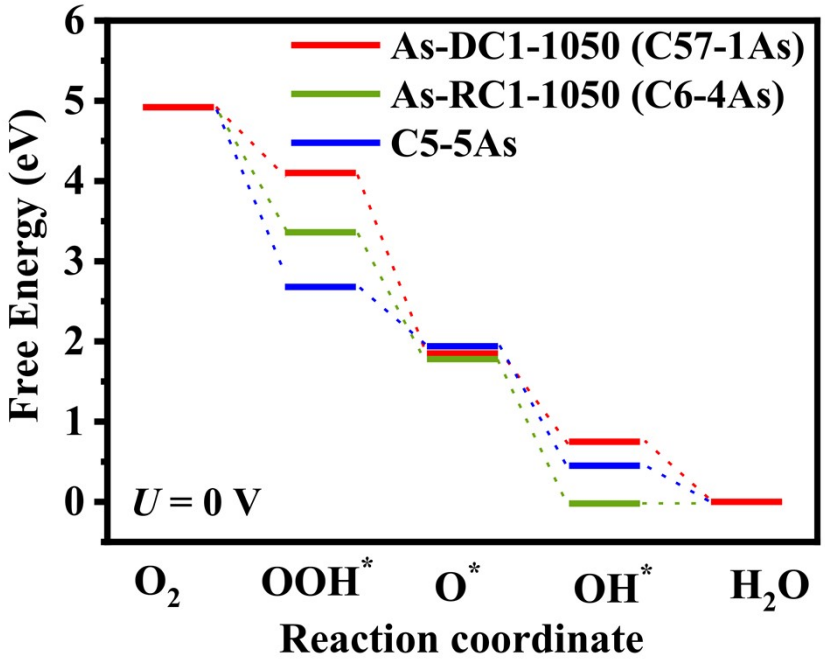

Figure S21. Free-energy diagrams and key reaction intermediates of C57-1As, C6-4As and C5-5As at U = 0 V. C57-1As exhibits the largest OH* adsorption free energy (ΔG_{OH}* = 0.75 eV) of the seven arsenic-based catalysts, indicating that the structure of C57-1As facilitates the desorption of OH* from the active site.

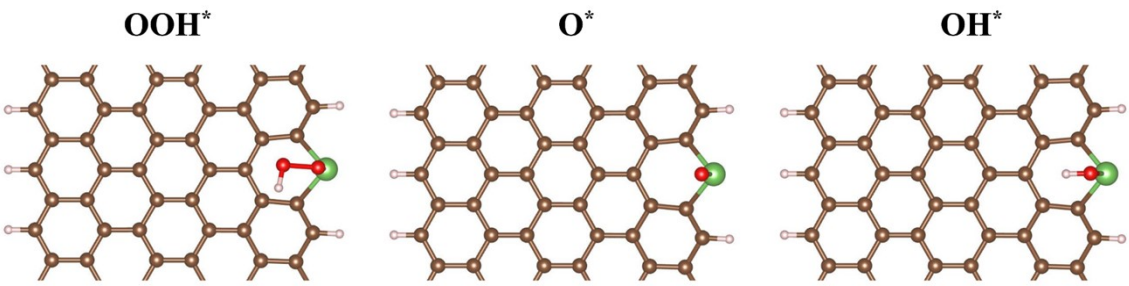

Figure S22. Optimized atomic configurations of three intermediates (OOH*, O*, and OH*) adsorbed on C6-4As.

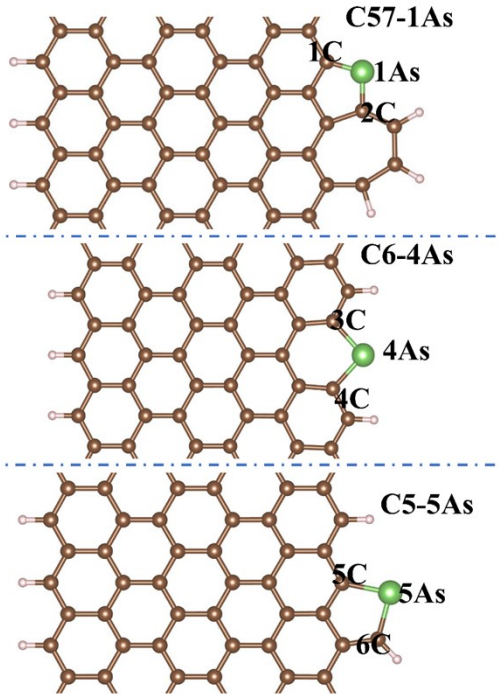

Sample	Atoms	Bader electrons	ΔQ
C57-1As	1As	4.424	-0.576
	1C	4.361	0.361
	2C	4.378	0.378
C6-4As	4As	4.324	-0.676
	3C	4.374	0.374
	4C	4.378	0.378
C5-5As	5As	4.405	-0.595
	5C	4.369	0.369
	6C	4.361	0.361

Figure S23. Bader charge analysis of C57-1As, C6-4As and C5-5As.

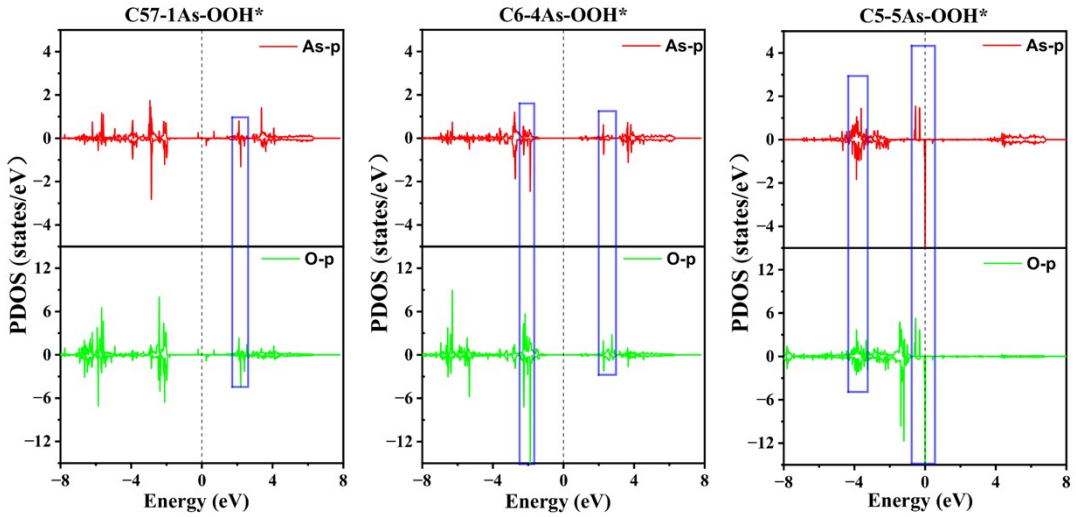

Figure S24. The projected density of states (PDOS) of C57-1As, C6-4As, and C5-5As. The Fermi level is set to zero, indicated by the black dashed line.

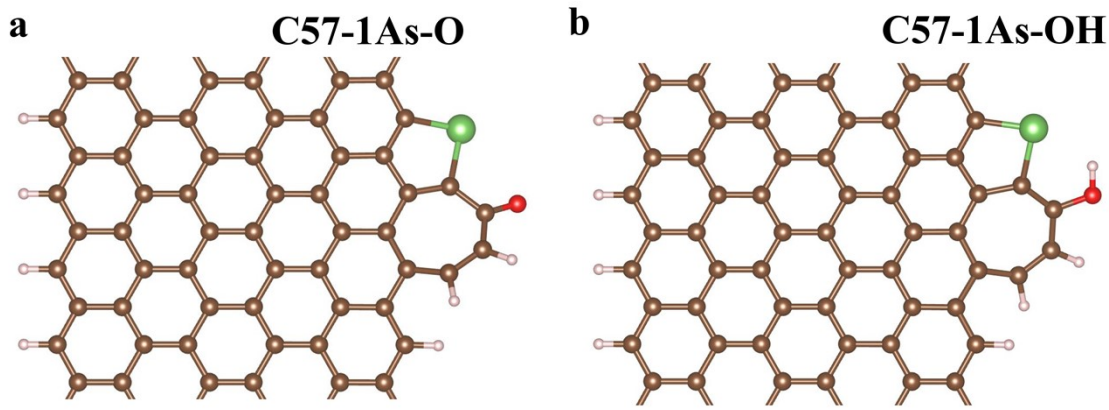

Figure S25. The models in which (a) oxygen and (b) hydroxyl groups located near C57-1As, respectively.

3. Supplementary Tables.

Table S1. The content of As, Se and I in the synthesized non-metal catalysts measured by ICP.

Sample	As-DC1-1050	As-RC1-1050	As-DC2-1050	Se-DC1-1050	I-DC1-1050	P-DC1-1050	Br-DC1-1050
content (wt%)	9.17%As	2.26% As	4.31% As	11.42% Se	13.78% I	9.61% P	12.57% Br

Table S2. EXAFS fitting results of As-DC1-1050 and As-RC1-1050.

Sample	Path	Coordination Number	Interatomic Distance (Å)	Debye-Waller factor（10^{-3} Å^2）	ΔE_0(eV)
As-RC1-1050	As-C	2.3±0.3	1.76±0.02	6.5±2.3	-1.15±0.6
As-DC1-1050	As-C	2.1±0.3	1.77±0.02	9.5±2.7	2.5±1.4

R factor is used to value the goodness of the fitting, R factor＜0.02. ΔE_0 is edge-energy shift (the difference between the zero kinetic energy value of the sample and that of the theoretical model).

Table S3. The content of dissolved As of As-DC1-1050, As-RC1-1050 and As-DC2-1050 measured by ICP.

Sample	After 10,000 cycles	After 20,000 cycles	After 35,000 cycles
As-DC1-1050	0.08 wt%	0.13 wt%	0.16 wt%
As-RC1-1050	0.07 wt%	0.11 wt%	0.15 wt%
As-DC2-1050	0.19 wt%	0.31 wt%	0.40 wt%

Table S4. Comparison of $E_{1/2}$ and onset potential of As-DC1-1050 with reported non-metal/non-precious metal catalysts in 0.1 M KOH.

Sample	E_{onset} (V vs RHE)	$E_{1/2}$ (V vs RHE)	Stability	Ref.
Se@NC-1000	0.95	0.85	negligible (5,000 cycles)	10
$N_{0.54}$-Z_3/M_1-900	0.96	0.825	current drop: 2.6% (24 h)	11
DG	0.91	0.76	-	9
NGM	0.89	0.77	current drop: 1.5% (8 h)	8
P-G	0.912	0.737	current drop: 12% (20,000 s)	12
NC@Co-NGC DSNCs	0.92	0.82	-	13
Fe-N_x/C	0.95	0.837	-	14
N-CNTs-650	0.94	0.85	current drop: 5% (40,000 s)	15
NPCN-900	0.92	0.78	current drop: 15.8% (12,000 s)	16
Carbon-L	0.86	0.7	current drop: 25% (25,000 s)	17
NDC-1000	0.96	0.86	-	18
FePhen@MOF-Ar NH3	1.03	0.86	current loss: 100 mA cm^{-2} (10,000 cycles)	19
NCNTFs	0.97	0.87	7 mV (5,000 cycles)	20
N-HC@G-900	1.0	0.85	negligible (10,000 cycles)	21
NPMC-1000	0.94	0.85	negligible (11,000 s)	22
N-GRW	0.92	0.84	15 mV (2,000 cycles)	23
SHG	1.01	0.87	current drop: 7% (100 h)	24
N-doped CNT arrays	0.91	0.8	-	25
Fe/SNC	＜1	0.86	current drop: 14% (3,000s)	26
Zn/CoN-C	1.004	0.861	12 mV (10,000 cycles)	27
As-DC1-1050	1.016	0.901	23 mV (35,000 cycles); 4 mV (35,000 cycles after re-calcination)	This work

Table S5. Summary of hydrogen-oxygen fuel cell performance.

Sample	Power density (mW cm^{-2})	Stability	Ref.
Fe-AC-CVD	601	current drop: 13% (319 h at 80 °C)	4
Pt_1-N/BP	680	current drop: 26% (200 h at 80 °C)	28
Fe/N/C-SCN	940	current drop: 71.88% (100 h at 80 °C)	29
Fe/N/C	-	current drop: 56% (100 h at 80 °C)	30
Zn/CoN-C	705	current drop: no attenuation (8 h)	27
Fe/PtCo-NC/TiO_x	952.2	current drop: 12.7% (150 h at 65 °C)	2
PFeTTPP-1000	730	current drop: ＞87.5% (100 h at 80 °C)	31
py-B12/C	370	current drop: 15% (100 h at 70 °C)	32
As-DC1-1050	701.9	current drop: 9.38% (290 h); 9.86% (590 h, re-calcination after 300 h at 65 °C)	This work

Table S6. Summary of Zinc-air battery performance.

Sample	Open circuit voltage (V)	Power density (mW cm^{-2})	Specific capacity (mAh g_{Zn}^{-1}; J=10 mA/cm^2)	Ref.
Fe-Se/NC	1.47	135	764	33
Se@NC-1000	1.45	176.9	801.3	10
Fe-N/P-C-700	1.42	133.2	723.6 (J=100)	34
D-CMO	1.46	149	-	35
IOSHs-NSC-Co_9S_8	1.497	133	738	36
SA-PtCoF	1.31	125	808	37
Fe-SAs/NPS-HC	1.45	195	-	38
FeNiCo@NC-P	1.36	112	807	39
FeP/Fe_2O_3@NPCA	1.42	130	717	40
FeNC-S-Fe_xC /Fe	1.41	149.4	663	41
S,N-Fe/N/C-CNT	1.25	102.7	-	42
Fe-N_x-C	1.49	96.4	641	43
As-DC1-1050	1.44	179.8	806.5	This work

Table S7. Adsorption free energies (eV) of OH, O and OOH over different active sites on As-C-based non-metal catalysts and carbon defect catalysts (U = 0 V).

Model	ΔG_{OH}*	ΔG_{O}*	ΔG_{OOH}*
C57-1As	0.75	1.85	4.1
C6-2As	-1.54	-0.65	1.94
C6-3As	-0.09	1.08	3.41
C6-4As	-0.02	1.78	3.36
C5-5As	0.45	1.94	2.68
C7-6As	-0.45	1.54	3.05
C57-7As	0.41	1.68	3.8
C57-8C	1.36	2.35	5.22
C57-9C	1.38	2.36	5.2

The four elementary steps of ORR as the following steps:

Step 1: $O_2 + H^+ + e^- + * \rightarrow OOH^*$

Step 2: $OOH^* + H^+ + e^- \rightarrow O^* + H_2O$

Step 3: $O^* + H^+ + e^- \rightarrow OH^*$

Step 4: $OH^* + H^+ + e^- \rightarrow * + H_2O$

Table S8. Adsorption free energies (eV) of OH, O and OOH over As site on As-DC1-1050 after oxidation (U = 0 V).

Model	ΔG_{OH}*	ΔG_{O}*	ΔG_{OOH}*
C57-1As	0.75	1.85	4.1
C57-1As-O	0.27	1.81	3.78
C57-1As-OH	1.02	0.98	4.28

Table S9. Difference in bond lengths (L) between adsorption behavior of OH* and OOH* on C57-1As, C57-1As-O and C57-1As-OH, respectively.

Model	$L_{O\text{-}O}$ of OOH* (Å)	$L_{O\text{-}As}$ of OH* (Å)
C57-1As	1.47	1.85
C57-1As-O	1.47	1.84
C57-1As-OH	1.48	1.86

The bond lengths of the adsorbed oxygen intermediates are not significantly different in the three models, indicating that differences in geometry are not a primary influence.

4. Supplementary References

1. L. Zhao, Y. Zhang, L. B. Huang, X. Z. Liu, Q. H. Zhang, C. He, Z. Y. Wu, L. J. Zhang, J. P. Wu, W. L. Yang, L. Gu, J. S. Hu and L. J. Wan, *Nat. Commun.*, 2019, **10**.
2. Y. J. Luo, Y. W. Wang, Y. Y. Wang, H. M. Huang, L. Zhang, H. J. Zhang and Y. Wang, *Appl. Catal. B-Environ.*, 2022, **317**.
3. R. J. Gao, J. Wang, Z. F. Huang, R. R. Zhang, W. Wang, L. Pan, J. F. Zhang, W. K. Zhu, X. W. Zhang, C. X. Shi, J. Lim and J. J. Zou, *Nat. Energy*, 2021, **6**, 614-623.
4. S. W. Liu, C. Z. Li, M. J. Zachman, Y. C. Zeng, H. R. Yu, B. Y. Li, M. Y. Wang, J. Braaten, J. W. Liu, H. M. Meyer, M. Lucero, A. J. Kropf, E. E. Alp, Q. Gong, Q. R. Shi, Z. X. Feng, H. Xu, G. F. Wang, D. J. Myers, J. Xie, D. A. Cullen, S. Litster and G. Wu, *Nat. Energy*, 2022, **7**, 652-663.
5. Z. Y. Jin, P. P. Li, Y. Meng, Z. W. Fang, D. Xiao and G. H. Yu, *Nat. Catal.*, 2021, **4**, 615-622.
6. G. Kresse and J. Hafner, *Phys Rev B Condens Matter*, 1993, **47**, 558-561.
7. J. P. Perdew, K. Burke and M. Ernzerhof, *Phys Rev Lett*, 1996, **77**, 3865-3868.
8. C. Tang, H. F. Wang, X. Chen, B. Q. Li, T. Z. Hou, B. S. Zhang, Q. Zhang, M. M. Titirici and F. Wei, *Adv. Mater.*, 2016, **28**, 6845-+.
9. Y. Jia, L. Z. Zhang, A. J. Du, G. P. Gao, J. Chen, X. C. Yan, C. L. Brown and X. D. Yao, *Adv. Mater.*, 2016, **28**, 9532-+.
10. H. Hu, J. J. Wang, B. F. Cui, X. R. Zheng, J. G. Lin, Y. D. Deng and X. P. Han, *Angew. Chem. Int. Ed.*, 2022, **61**.
11. X. G. Li, B. Y. Guan, S. Y. Gao and X. W. Lou, *Energ. Environ. Sci.*, 2019, **12**, 648-655.
12. L. Tao, Q. Wang, S. Dou, Z. L. Ma, J. Huo, S. Y. Wang and L. M. Dai, *Chem Commun*, 2016, **52**, 2764-2767.
13. S. H. Liu, Z. Y. Wang, S. Zhou, F. J. Yu, M. Z. Yu, C. Y. Chiang, W. Z. Zhou, J. J. Zhao and J. S. Qiu, *Adv. Mater.*, 2017, **29**.
14. N. Ramaswamy, U. Tylus, Q. Y. Jia and S. Mukerjee, *J. Am. Chem. Soc.*, 2013, **135**, 15443-15449.
15. J. S. Meng, C. J. Niu, L. H. Xu, J. T. Li, X. Liu, X. P. Wang, Y. Z. Wu, X. M. Xu, W. Y. Chen, Q. Li, Z. Z. Zhu, D. Y. Zhao and L. Q. Mai, *J. Am. Chem. Soc.*, 2017, **139**, 8212-8221.
16. H. Jiang, Y. Q. Wang, J. Y. Hao, Y. S. Liu, W. Z. Li and J. Li, *Carbon*, 2017, **122**, 64-73.
17. P. Zhang, F. Sun, Z. H. Xiang, Z. G. Shen, J. Yun and D. P. Cao, *Energ. Environ. Sci.*, 2014, **7**, 442-450.
18. Q. X. Lai, J. Zheng, Z. M. Tang, D. Bi, J. X. Zhao and Y. Y. Liang, *Angew. Chem. Int. Ed.*, 2020, **59**, 11999-12006.
19. K. Strickland, M. W. Elise, Q. Y. Jia, U. Tylus, N. Ramaswamy, W. T. Liang, M. T. Sougrati, F. Jaouen and S. Mukerjee, *Nat. Commun.*, 2015, **6**.
20. B. Y. Xia, Y. Yan, N. Li, H. B. Wu, X. W. Lou and X. Wang, *Nat. Energy*, 2016, **1**.

21. J. Sun, S. E. Lowe, L. J. Zhang, Y. Z. Wang, K. L. Pang, Y. Wang, Y. L. Zhong, P. R. Liu, K. Zhao, Z. Y. Tang and H. J. Zhao, *Angew. Chem. Int. Ed.*, 2018, **57**, 16511-16515.
22. J. T. Zhang, Z. H. Zhao, Z. H. Xia and L. M. Dai, *Nat. Nanotechnol.*, 2015, **10**, 444-452.
23. H. B. Yang, J. W. Miao, S. F. Hung, J. Z. Chen, H. B. Tao, X. Z. Wang, L. P. Zhang, R. Chen, J. J. Gao, H. M. Chen, L. M. Dai and B. Liu, *Sci Adv*, 2016, **2**.
24. C. G. Hu and L. M. Dai, *Adv. Mater.*, 2017, **29**.
25. K. P. Gong, F. Du, Z. H. Xia, M. Durstock and L. M. Dai, *Science*, 2009, **323**, 760-764.
26. H. J. Shen, E. Gracia-Espino, J. Y. Ma, K. T. Zang, J. Luo, L. Wang, S. S. Gao, X. Mamat, G. Z. Hu, T. Wagberg and S. J. Guo, *Angew. Chem. Int. Ed.*, 2017, **56**, 13800-13804.
27. Z. Y. Lu, B. F. Wang, Y. F. Hu, W. Liu, Y. F. Zhao, R. O. Yang, Z. P. Li, J. Luo, B. Chi, Z. Jiang, M. S. Li, S. C. Mu, S. J. Liao, J. J. Zhang and X. L. Sun, *Angew. Chem. Int. Ed.*, 2019, **58**, 2622-2626.
28. J. Liu, M. G. Jiao, L. L. Lu, H. M. Barkholtz, Y. P. Li, Y. Wang, L. H. Jiang, Z. J. Wu, D. J. Liu, L. Zhuang, C. Ma, J. Zeng, B. S. Zhang, D. S. Su, P. Song, W. Xing, W. L. Xu, Y. Wang, Z. Jiang and G. Q. Sun, *Nat. Commun.*, 2017, **8**.
29. Y. C. Wang, Y. J. Lai, L. Song, Z. Y. Zhou, J. G. Liu, Q. Wang, X. D. Yang, C. Chen, W. Shi, Y. P. Zheng, M. Rauf and S. G. Sun, *Angew. Chem. Int. Ed.*, 2015, **54**, 9907-9910.
30. M. Lefevre, E. Proietti, F. Jaouen and J. P. Dodelet, *Science*, 2009, **324**, 71-74.
31. S. W. Yuan, J. L. Shui, L. Grabstanowicz, C. Chen, S. Commet, B. Reprogle, T. Xu, L. P. Yu and D. J. Liu, *Angew. Chem. Int. Ed.*, 2013, **52**, 8349-8353.
32. S. T. Chang, C. H. Wang, H. Y. Du, H. C. Hsu, C. M. Kang, C. C. Chen, J. C. S. Wu, S. C. Yen, W. F. Huang, L. C. Chen, M. C. Lin and K. H. Chen, *Energ. Environ. Sci.*, 2012, **5**, 5305-5314.
33. Y. Wang, J. Wu, S. H. Tang, J. R. Yang, C. L. Ye, J. Chen, Y. P. Lei and D. S. Wang, *Angew. Chem. Int. Ed.*, 2023, DOI: 10.1002/anie.202219191.
34. K. Yuan, D. Lutzenkirchen-Hecht, L. B. Li, L. Shuai, Y. Z. Li, R. Cao, M. Qiu, X. D. Zhuang, M. K. H. Leung, Y. W. Chen and U. Scherf, *J. Am. Chem. Soc.*, 2020, **142**, 2404-2412.
35. F. Yang, J. H. Xie, D. W. Rao, X. Q. Liu, J. X. Jiang and X. H. Lu, *Nano Energy*, 2021, **85**.
36. K. Tang, C. Z. Yuan, Y. Xiong, H. B. Hu and M. Z. Wu, *Appl. Catal. B-Environ.*, 2020, **260**.
37. Z. li, W. H. Niu, Z. Z. Yang, N. Zaman, W. Samarakoon, M. Y. Wang, A. Kara, M. Lucero, M. V. Vyas, H. Chao, H. Zhou, G. E. Sterbinsky, Z. X. Feng, Y. G. Du and Y. Yang, *Energ. Environ. Sci.*, 2020, **13**, 884-895.
38. Y. J. Chen, S. F. Ji, S. Zhao, W. X. Chen, J. C. Dong, W. C. Cheong, R. A. Shen, X. D. Wen, L. R. Zheng, A. I. Rykov, S. C. Cai, H. L. Tang, Z. B. Zhuang, C. Chen, Q. Peng, D. S. Wang and Y. D. Li, *Nat. Commun.*, 2018, **9**.
39. D. Z. Ren, J. Ying, M. L. Xiao, Y. P. Deng, J. H. Ou, J. B. Zhu, G. H. Liu, Y. Pei,

S. Li, A. M. Jauhar, H. L. Jin, S. Wang, D. Su, A. P. Yu and Z. W. Chen, *Adv. Funct. Mater.*, 2020, **30**.
40. K. Z. Wu, L. Zhang, Y. F. Yuan, L. X. Zhong, Z. X. Chen, X. Chi, H. Lu, Z. H. Chen, R. Zou, T. Z. Li, C. Y. Jiang, Y. K. Chen, X. W. Peng and J. Lu, *Adv. Mater.*, 2020, **32**.
41. Y. Y. Qiao, P. F. Yuan, Y. F. Hu, J. N. Zhang, S. C. Mu, J. H. Zhou, H. Li, H. C. Xia, J. He and Q. Xu, *Adv. Mater.*, 2018, **30**.
42. P. Z. Chen, T. P. Zhou, L. L. Xing, K. Xu, Y. Tong, H. Xie, L. D. Zhang, W. S. Yan, W. S. Chu, C. Z. Wu and Y. Xie, *Angew. Chem. Int. Ed.*, 2017, **56**, 610-614.
43. J. X. Han, X. Y. Meng, L. Lu, J. J. Bian, Z. P. Li and C. W. Sun, *Adv. Funct. Mater.*, 2019, **29**.